

Supporting Information

Design of charge transporting grids for efficient ITO-free flexible large area organic photovoltaics

Lijian Zuo, Shuhua Zhang, Minmin Shi, Hanying Li, and Hongzheng Chen**

Experimental Section

Materials: All the materials are from Sigma Aldrich Corp. if without specification. The PTB7, PTB7-Th, PFN, and PC₇₁BM are from 1-Materials Corp, and used as received.

OSC device fabrication: Glass substrates were cleaned in detergent, acetone, and isopropanol sequentially by ultra-sonic. These substrates were treated by the UV-Ozone machine for 15 min before depositing 200 nm Ag in the vacuum chamber. Then, 10 nm PFN layer is processed from a methanol solution onto the Ag film and annealed at 120°C for 5 min in glove-box. After cooling down to room temperature, a solution of PTB7:PC₇₁BM or PTB7-Th:PC₇₁BM blends (1:1.5 wt% and 25 mg/ml in total) were spin-casted from the chlorobenzene (mixed with 3% 1,8-diiodooctane in vol%) onto the PFN layer, which afford a film of 70-80 nm as measured by atomic force microscope (AFM, veeco IIIa). The substrates were again transferred into the vacuum chamber for deposition of 10 nm MoO₃ as hole selective transport layer, different thickness Ag as TE, and 50 nm MoO₃ as capping layer below 4×10⁻⁴ pa, sequentially. For large area OSC, the charge collecting grids were inserted immediately after deposition of the ultra-thin Ag layer.

OSC device measurement: The R_{sheet} of the TE was measured by a four points probe. The OPV device I-V characteristics is recorded on a Keithley 2400 source meter under a 1 sun, AM 1.5G spectrum from a solar simulator with intensity calibrated by a standard silicon diode, which was certified at National Renewable Energy Lab (NREL).

Optical simulation: The optical simulations based on the transfer matrix formalism (TMF)¹ are used to calculate the interference of reflected and transmitted light at each interface within the stratified devices. The wavelength-dependent optical properties of each layer is represented by the index of refraction ($\tilde{n} = n + ik$) of each material, acquired by variable angle spectroscopic ellipsometry (VASE). All the simulations are based on the assumptions of planar interfaces and total isotropy for all layers. However, the interference within the glass substrates is ignored because their thicknesses (2 mm) are much higher than the wavelengths of the simulated incident beams. For each device structure, the optical simulation adopts exactly the same layer thickness as those used in practical device fabrication. In addition, 100% internal quantum efficiency and the AM1.5 intensity spectrum (ASTM G173-03) are assumed to calculate the theoretically maximum photocurrent density.

Resistive energy loss calculation: The details for deduction of each equation for both thermal dissipation and the bias-voltage drop follows our previous work.^[2]

Table S1. Summary of current status of literature reported large area organic solar cells.

Device area (cm ²)	structures	Efficiency (%)	Retention ratio	ref
7	monolithic	0.41	33%	<i>J. Appl. Phys.</i> 2009, 106, 054507.
7	with grid	0.77	62%	<i>J. Appl. Phys.</i> 2009, 106, 054507.
1.2	with grid	5.85	97%	<i>Nano Energy</i> (2014) 10, 259–267
2.9	monolithic	3.90	87%	<i>Adv. Mater.</i> 2012, 24, 2572–2577
25	monolithic	3.08	70%	<i>Adv. Mater.</i> 2012, 24, 2572–2577
25	monolithic	2.20	34%	<i>Adv. Energy Mater.</i> 2014, 1401221
25	with grids	4.61	72%	<i>Adv. Energy Mater.</i> 2014, 1401221

7	with grid	0.81	67%	<i>Optics Express 2010, 18, A459</i>
--	sub-module	5.61	90%	<i>Adv. Mater. 2014, 26, 1602–1606</i>
12.3	grid	2.11	67%	<i>Sol. Energ. Mater. Sol. C. 2011, 95</i> <i>852–855</i>
4	gradient electrode	7.15	80%	<i>Adv. Mater. 2015, 27, 6983–6989</i>
4.2	sub-module	7.5%	90%	<i>Nat. Comm. 2015,</i> <i>doi:10.1038/ncomms10279</i>
4	triangular grid	short 6.93	79%	<i>this work</i>

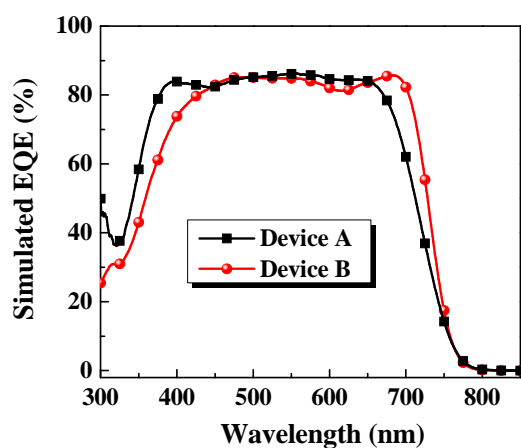


Figure S1. Simulated light absorbing fraction (or simulated external quantum efficiency assuming 100% internal quantum efficiency) spectra of PTB7:PC71BM active layer in device A and device B.

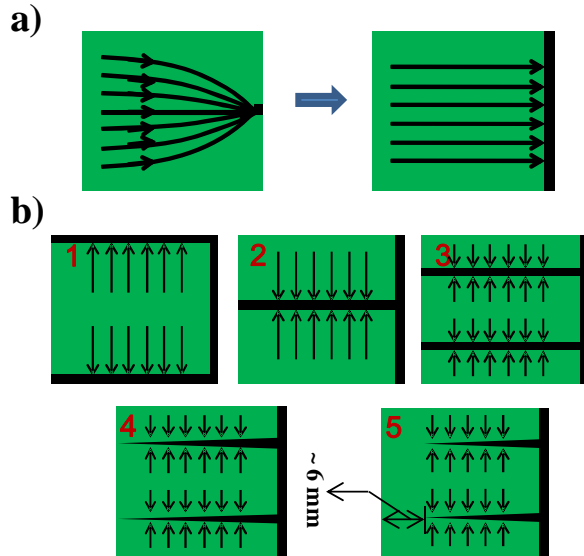


Figure S2. a) Schematic diagram of variation in the current flow on the transparent electrode sheet without and with the bottom charge collecting grid. **b)** schematic diagram of charge transporting grid with different patterns and current flow directions on them. The deposition of CT-grids decreases the charge transporting distance, and alters the charge flow direction on the sheet of the ultra-thin Ag TE as shown in **Figure 4b**. Without CT-grids, current flows have to go through the large transparent sheet before being collected by the CC-grid, while with the CT-grid, the photo-current would flow to the CT-grids first and then to the CC-grid to be collected. Thereafter, the photo current flow pathways especially for that generated far away from the CC-grids of the large area sheet is significantly reduced. As observed, introducing two side CT-grids (grid 1) improves both the J_{SC} and the overall device PCE to the maximum of 4.88%, at the cost of $\sim 10\%$ shadow loss. The increased PCE can be attributed to the shortened current flow distance as shown in **Figure 4b**. Due to the existence of the two side highly conductive grids, the photo currents generated far away from the bottom CC-grid tend to transport to the side grids, and then to the bottom grids, leading to energy loss reduction. To reduce the shadow loss, we deposit only one CT-grid in the middle (grid 2). The grid 2 shows similar effect to shorten the current flow distance compared with grid 1, but reduces the shadow loss by 50%. The corresponding device performances show the

same trend, and the J_{SC} s show appreciable increase from 12.87 to 13.12 mA/cm². To further reduce the current flow distance, two CT-grids on the ultra-thin Ag are deposited (grid 3). As shown, the denser CT-grid distribution further shortens the charge transporting distance and the corresponding energy loss is reduced. Thereafter, although the grid 3 has larger shadow loss compared with that of grid 2, the J_{SC} is increased, which is attributed to the reduced thermal dissipation loss and the reduced bias voltage induced energy loss associated with the shortened charge transporting distance. As a result, the device performance is further improved to 5.42%, with the best device performance up to 6.04%.

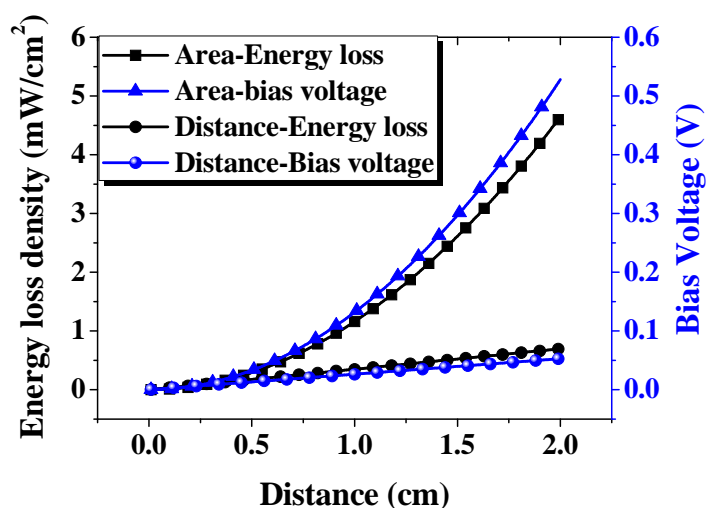


Figure S3. Calculated energy loss density, and bias voltage drop for large area organic solar cells with different device areas and different charge transporting distances. (the R_{sheet} of the 12 nm Ag is $\sim 10 \Omega/\square$, the J_{max} of the OSC device is 13.5 mA/cm², details for the calculation can be found in our previous work^[2]).

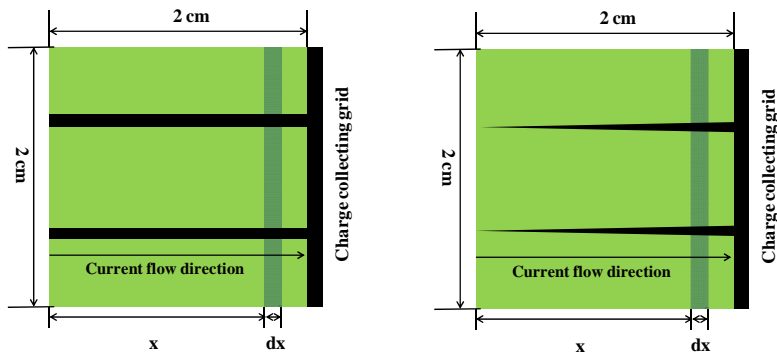


Figure S4. The schematic diagram of device architecture for the energy loss density profile calculation (bottom, left: grid 3, right: grid 4). The boundary conditions for calculation include: the R_{sheet} of the CT-grid is estimated to be $\sim 0.018 \Omega/\square$, the J_{max} of the OSC device is $\sim 12.0 \text{ mA}/\text{cm}^2$. The averaged energy loss on the charge transporting grids is calculated to be $0.034 \text{ mW}/\text{cm}^2$ for grid 3 (left) and $0.049 \text{ mW}/\text{cm}^2$ for grid 4. Both of the energy loss densities are marginal compared to the energy conversion power of $\sim 8 \text{ mW}/\text{cm}^2$ for small area device under AM 1.5 G 1 sun illumination, indicating that changing the grid structure from rectangular to triangular would not influence the overall device performance obviously.

Simulation of resistive energy loss on large area organic solar cells ($10 \times 10 \text{ cm}^2$ square):

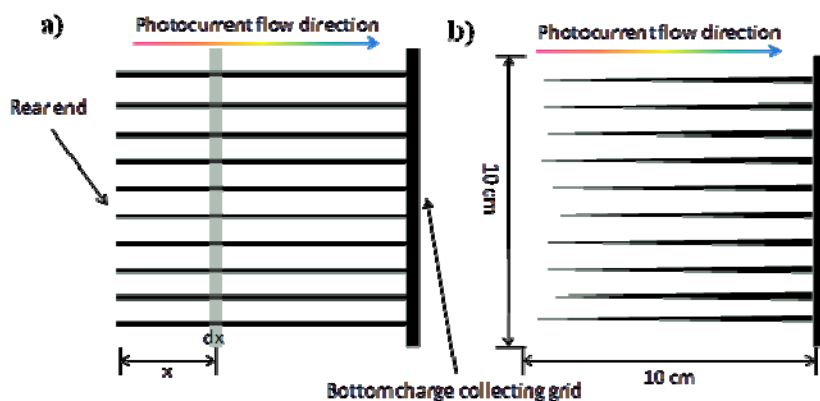


Figure S5. Schematic diagram of the 100 cm^2 large area organic solar cells with different grid design: a) traditional rectangular grid structures, b) novel triangular grid patterns.

We assuming that, the energy loss caused with the current flowing to the grids is negligible, and the one dimensional model should also hold true along each grids. The boundary conditions include: J_{\max} is 12 mA/cm², width of the rectangular grid is 1 mm, which compose 10% shadow loss for the rectangular structured grid and 5% for the triangular structured grid.

The Joule's equation depicting the thermal dissipation energy loss is:

$$W = I^2 R \quad (1)$$

Where, the W is the thermal dissipation energy loss on the transparent electrode, I is the photo-current flow across the transparent electrode, and R is the resistance of the transparent electrode. Since the photo-current flow show gradient distribution across grids, we calculate the total energy loss on the grids by integrating the energy loss on each pixel on the grids of large area solar cells. As a result, the photocurrent and resistance on x position of the grid should be:

$$I = JA = J \times (x \times d) / n \quad (2)$$

Where, I is the photocurrent flow on each grid at x position, J is the maximum point photocurrent density (J_{\max}), A is the area from the rear end to the x position of the large area transparent sheet, x is the distance from the rear end of the device to the x position, the d is the width of the device, which is 10 cm in our case, and the n is numbers of the grids, which is 10.

$$R = R_{sheet} \times \frac{dx}{a} \quad (3)$$

Where, R is the resistance of the rectangular grid on pixel x, R_{sheet} is the sheet resistance of the grids, a is the width of the grids, which is 0.1 cm, and the dx is the length of pixel x of the grids. Thereafter, the energy loss on pixel x can be described as:

$$dW = I^2 \times R = \left[J \times \frac{x \times d}{n} \right]^2 \times R_{sheet} \times \frac{dx}{a} \quad (4)$$

And the energy loss on one of the grids is:

$$W_1 = \int_0^{10} dW = \int_0^{10} I^2 \times R = \left[J \times \frac{x \times d}{n} \right]^2 \times R_{sheet} \times \frac{dx}{a} = \int_0^{10} J^2 \times x^2 \times R_{sheet} \times 10 dx \quad (5)$$

On a $10 \times 10 \text{ cm}^2$ large area organic solar cells with rectangular grid design, the energy loss on 1 grid should be:

$$W_1 = 0.48 \times R_{sheet} \quad (6)$$

And the averaged energy loss density on the 100 cm^2 large area sheet caused by the 10 grids should be

$$E_{avg} = \frac{W_{total}}{100 \text{ cm}^2} = 0.048 \times R_{sheet} \text{ W/cm}^2 \quad (7)$$

Where, W_{total} is the total energy loss on the 10 grids.

Considering the 1 sun AM 1.5G intensity of 100 mW/cm^2 , and the power conversion efficiency of 8.09%, the averaged power generation density is 8.09 mW/cm^2 . In order to make sure the average energy loss density caused by the grids is less than 1% of the averaged power generation density, the R_{sheet} of the grid should be $0.0017 \Omega/\square$.

Thereafter, with the grid sheet resistance of $0.0017 \Omega/\square$, J_{max} of 12 mA/cm^2 , and rectangular grid structure design, the large area organic solar cells with the shadow loss of 10%, resistive loss of 1% , and the total energy loss of 11% can be achieved. In order to evaluate the effectiveness of our designed grid structures (the triangular structure grids) on large area organic solar cells of 100 cm^2 , we calculated the optical energy loss and the resistive energy loss with the same boundary condition as those for the rectangular structured grid patterns. Compared to the rectangular grid, the only difference with the triangular grid is the resistance on pixel x:

$$R = R_{sheet} \times \frac{dx}{l(x)} \quad (8)$$

Where, $l(x)$ is the width of the grid at x position, which can be expressed as follow:

$$l(x) = \frac{x}{10} \text{ cm} \quad (9)$$

Where, x is the length from the rear end to the x position, 10 cm is the total length of the grid. Thereafter, the energy loss on each grids can be described as:

$$W_1 = \int_0^{10} dW = \int_0^{10} I^2 \times R = \int \left[J \times \frac{x \times d}{n} \right]^2 \times R_{sheet} \times \frac{10 \times dx}{x \times x} = 100 \int_0^{10} J^2 \times R_{sheet} dx \quad (10)$$

On a $10 \times 10 \text{ cm}^2$ large area organic solar cells with rectangular grid design, the energy loss on 1 grid should be:

$$W_1 = 0.72 \times R_{\text{sheet}} \quad (11)$$

Thereafter, the average resistive energy loss density caused by the grid structures can be described as:

$$R_{\text{ave.}} = \frac{W_{\text{total}}}{100 \text{ cm}^2} = 0.072 \times R_{\text{sheet}} \text{ W/cm}^2 = 0.121 \text{ mW/cm}^2 \quad (12)$$

Thereafter, the averaged resistive energy loss caused by the triangular structured grid pattern is 0.121 mW/cm^2 , which constitutes 1.5% compared to the power generation density for the organic solar cells under 1 sun intensity. The optical loss of the triangular structured grid pattern reduced 50% compared to the rectangular structured solar cells, and the optical loss is only 5% compared to power generation density. As a result, the total energy loss density with the triangular grid design is merely 6.5%, which is significantly reduced compared to the rectangular structured grid (11%). With the calculation results, it is very obvious that the triangular structure grid design show advantages over the traditional rectangular structured grid patterns. We note that the energy loss is closely associated with the grid sheet resistance (equation 7,12). The lower the resistance is (e.g., with thicker grids), the more significantly the triangular structure will exhibit its advantage.

Designed grid pattern by integrating the conductance gradient strategy to the hexagonal structured patterns:

We propose the novel design combining the merits of both of the grids, which is illustrated in **Figure 2**. The width of the grids and the area of each hexagonal unit determines the optical loss, and by taking the gradient energy loss into consideration, we proposed the hexagonal structures pattern with the width of the grids gradually increasing along the photocurrent flow

direction. By this design, we can reduce the optical loss, while keep the resistive energy loss similar to the traditional hexagonal pattern.

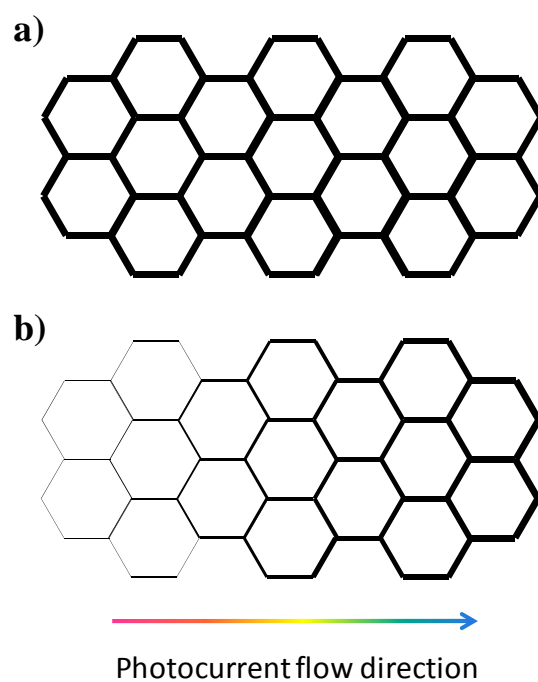


Figure S6. a) traditional hexagonal structure charge transporting grids, b) novel hexagonal structure grids design with gradient conductance structure.

References

- 1 G. F. Burkhard, E. T. Hoke, M. D. McGehee, *Adv. Mater.* **22**, 3293-3297 (2010).
- 2 L. Zuo, S. Zhang, H. Li, H. Chen, *Adv. Mater.* **27**, 6983-6989(2015).